

Biochemistry. Author manuscript; available in PMC 2012 February 22.

Published in final edited form as:

Biochemistry. 2011 February 22; 50(7): 1226–1237. doi:10.1021/bi101432p.

Improving a designed photo-controlled DNA-binding protein

Helen Y. Fan[†], Stacy-Anne Morgan, Katherine E. Brechun, Yih-Yang Chen[†], Anna S. I. Jaikaran, and G. Andrew Woolley

G. Andrew Woolley: awoolley@chem.utoronto.ca

[†] Faculty of Engineering, University of Waterloo 200 University Avenue West, Waterloo, Ontario, Canada N2L 3G1 and Department of Chemistry, University of Toronto, 80 St. George St., Toronto, ON, M5S 3H6, Canada

* Department of Chemistry, University of Toronto, 80 St. George St., Toronto, ON, M5S 3H6, Canada, telephone: (416) 978-0675 fax: (416) 978-8775

Abstract

Photo-controlled transcription factors could be powerful tools for probing the roles of transcriptional processes in a variety of settings. Previously, we designed a photo-controlled DNA binding protein based on a fusion between the bZIP region of GCN4 and photoactive yellow protein from H. halophila (Morgan et al., J. Mol. Biol. 2010, 399:94-112). Here we report a structure-based attempt to improve the degree of photoswitching observed with this chimeric protein. Using computational design tools PoPMuSiC 2.0, Rosetta, Eris and bCIPA we identified a series of single and multiple point mutations that were expected to stabilize the folded dark state of the protein and thereby enhance the degree of photoswitching. While a number of these mutations, particularly those that introduced a hydrophobic residue at position 143, did significantly enhance dark-state protein stability as judged by urea denaturation studies, dark-state stability did not correlate directly with the degree of photoswitching. Instead, the influence of mutations on the degree of photoswitching was found to be related to their effects on the degree to which DNA binding slowed the pB to pG transition in the PYP photocycle. One mutant, K143F, caused a ~10fold slowing of the photocycle and also showed the largest difference in apparent K_d for DNA binding – 3.5-fold lower upon irradiation. This change in apparent K_d causes a 12-fold enhancement in fraction bound DNA upon irradiation due to the cooperativity of DNA binding by this family of proteins. The results highlight the strengths and weaknesses of current approaches to a practical problem in protein design as well as suggesting strategies for further improvement of designed photo-controlled transcription factors.

Keywords

coiled-coil; bZIP; photo-control; photoactive yellow protein; PYP; optogenetics; photoisomerization; genetically encoded; LOV domain

Photo-control of transcriptional processes in living cells may help to elucidate the roles of location and timing of gene expression in spatiotemporally complex settings such as occur during development and during normal functioning of the nervous system (1). Naturally occurring photo-controlled transcription factors are known (2,3), however, they are often multi-component systems so that engineering them for use as tools for the photo-control of transcription is not straightforward. Alternatively, naturally occurring light-dependent protein-protein interactions may be co-opted to photo-control transcription. Quail and

colleagues used a phytochrome-GAL4-DNA-binding-domain fusion and a PIF3-GAL4-activation-domain fusion to photo-control the expression of genes that contain a promoter with a GAL4 binding site (4). A similar approach using the transactivator VP16 fused to the LOV domain of FKF1 and the partner protein GIGANTEA fused to the GAL4 DNA binding domain has been reported by Yazawa et al (5). In an elegant, structure-based approach to the creation of a light-activated DNA binding protein, Strickland *et al* linked a LOV domain to the Trp repressor via a shared α -helix (6,7). In their design, the helix is expected to be packed against the LOV domain in the dark and thus cannot adopt its normal location in the Trp repressor, inhibiting Trp repressor DNA binding ability. Upon irradiation, the helix detaches from the LOV domain to rejoin the Trp repressor thereby activating it.

We recently reported a conceptually similar design of a photo-controlled bZIP type DNAbinding protein (GCN4Δ25PYP-v2) that is a hybrid of the prototypical homodimeric bZIP DNA-binding protein GCN4 and photoactive yellow protein (PYP), a blue light sensitive protein from Halorhodospira halophila (8). A fusion of the C-terminal coiled-coil region of GCN4 bZIP with the N-terminal cap of PYP was made based on examination of available crystal structure data, analysis of amino acid preference rules for coiled-coils, mutational and amino acid conservation data for PYP together with Rosetta-guided structural modeling. GCN4Δ25PYP-v2 is monomeric in the dark and fluorescence and circular dichroism data indicate the coiled-coil domain is hidden. Binding to target DNA in the dark causes substantial structural reorganization of GCN4Δ25PYP-v2 with a concomitant slowing of the photocycle consistent with conformational coupling of the DNA-binding and light-sensitive domains of the protein. Blue light irradiation caused a 2-fold decrease in the apparent K_d for specific DNA binding that reversed in the dark. Although this effect was reproducible and reversible, a more substantial difference in DNA binding between dark and light states would be preferable if such designs are to be useful as tools for controlling DNA binding and transcription in vivo.

If a suitable selection or screening approach were devised, random mutagenesis might be expected to yield GCN4 Δ 25PYP variants with improved photoswitching behavior. A consequence of the structure-based approach, however, is that the structure may help narrow the search for proteins with improved properties. Here we focus on efforts to stabilize the hybrid N-terminal cap of GCN4 Δ 25PYP-v2 in its dark state by seeking to optimize packing interactions between the hybrid cap and its docking sites on the PYP core with the anticipation that this may lead to larger differences in DNA binding upon irradiation. Stabilization of a well defined folded structure by targeted mutation is a task considered amenable to computational modeling techniques (9,10). Here we have used several such computational approaches to design a small set of GCN4 Δ 25PYP variants. These proteins were then expressed and their dark state stability as well as their photoswitching behavior characterized in detail.

Materials and Methods

Site directed mutagenesis

Primers for the mutations were designed with PrimerX (http://www.bioinformatics.org/primerx/) following the Stratagene QuikChange protocol (Agilent, Inc.) and purchased from ACGT Corp. For each mutation, 125 ng of each the forward and reverse primers were added to 100 ng of template DNA, 1 μ L of dNTPs, 5 μ L DMSO, 1 μ L Pfu polymerase (Fermentas), 5 μ L 10× Pfu reaction buffer with MgSO₄, and water to a total volume of 50 μ L. A drop of mineral oil was also added to prevent evaporation. The reaction mixture was held at (i) 95°C for 30 seconds followed by (ii) 30 seconds at 95°C, (iii) 1 minute at 5°C below primer T_m and (iv) 7.5 minutes at 72°C. Steps (ii)–(iv) were repeated 18 times. Then the mixture was held at (v) 72°C for an additional 20

minutes before being allowed to cool to room temperature. A 1 μ L aliquot of DpnI was added to the reaction mixture which was then incubated at 37°C for one hour. A 0.8% agarose gel in 0.5× TBE was then run to check for PCR products. A PCR purification kit (Invitrogen) was subsequently used and the product was transformed into XL-2 Blue Ultracompetent cells. A midiprep (Invitrogen) was carried out and the plasmids were sequenced in both directions (ACGT Corp.) to confirm the mutations.

Protein expression and purification

The expression and reconstitution of the PYP constructs were adapted from the work of Devanathan *et al* (11). The protocol was the same for all constructs. DNA (0.2 ng) was transformed into BL21*(DE3) competent cells and plated onto agar plates containing 30 µg/mL kanamycin. The following day, a single colony was used to inoculate 25 mL of Luria-Bertani (LB) broth that had been supplemented with kanamycin (30 µg/mL) and grown overnight at 37 °C. The 25 mL overnight culture was subsequently used to inoculate 1 L of LB supplemented with 30 µg/mL kanamycin. Cells were grown at 37°C until an O.D. of 0.6 was reached and then induced with 1 mM IPTG. The temperature was adjusted to 25 °C and the cells grown for a further 1.5 hrs before 30 mg of activated chromophore dissolved in 1 mL of ethanol was added to the media. The synthesis of the activated chromophore, 4-hydroxycinnamic acid thiophenyl ester, was carried out as detailed by Changenet-Barret *et al.* (12) except that the product used for the reconstitution of holoprotein was not recrystallized. The cells were grown for a further 6 hours before centrifugation to separate the media from the protein-containing cell pellet.

The pellet was resuspended in buffer containing 50 mM sodium phosphate, pH 8.0, 300 mM sodium chloride and 5 mM magnesium chloride and frozen at -20° C until purification. The resuspended cell pellet was sonicated in pulses on ice for 5 min and then centrifuged at 18K for 30 min to separate the supernatant from the pellet. The protein was purified on a Ni-NTA column that was equilibrated with the lysis buffer. After addition of the protein-containing supernatant, the resin was washed with 10 column volumes (CV) of the lysis buffer. The resin was subsequently washed with 5 CVs of high salt buffer (*i.e.* lysis buffer supplemented with 2 M NaCl) followed by a further 5 CVs of lysis buffer. To elute non-specifically bound proteins, the resin was subjected to 5 CVs of lysis buffer supplemented with 5 mM imidazole. The protein was eluted by increasing the concentration of imidazole to 200 mM.

The eluted protein was dialyzed extensively against 40 mM Tris.OAc, 1 mM EDTA, 100 mM NaCl, pH 7.5 ($1\times$ TAE, 100 mM NaCl, pH 7.5). The dialyzed protein was concentrated to ~1.5 mL using an Amicon ultracentrifugal device (10,000 Da NMWL) (Millipore). The purity of the samples was confirmed using 12.5% SDS-PAGE and ESI-MS. Where further purification was required, the protein was applied to a Superdex 75 column running in $1\times$ TAE, 100 mM NaCl, pH 7.5 at 4°C. UV-Vis absorbance spectroscopy was used to determine which eluted fractions had the highest ratios of the absorbance at 446 nm to that at 278 nm.

Target DNA

The following oligomers were used for annealing AP-1 duplexes: AP1_S1: 5′ TCC GGA TGA CTC ATT TTT TG 3′; Cy3_AP1_S1: 5′ Cy3 - TCC GGA TGA CTC ATT TTT TG 3′; AP1_S2: 5′ CAA AAA ATG AGT CAT CCG GA 3′. A 1:1 ratio of each unlabelled oligonucleotide in 10 mM Tris.HCl, 50 mM NaCl, 1 mM EDTA, pH 7.6 was heated in a water bath to 80°C for 10 min. After 10 min, the hot plate was turned off and the DNA allowed to slowly cool to room temperature. For labeled AP-1 DNA, a 1:1.2 ratio of labeled to unlabelled oligonucleotide was used.

UV-Vis spectra and Photoisomerization

UV-Vis spectra of the proteins were obtained in 1x TAE, 100 mM NaCl, pH 7.5 at 20°C in a 1.0 cm path length quartz cuvette using a PE Lambda 35 spectrophotometer. Protein concentrations were determined using an extinction coefficient at λ_{max} (~446 nm) of 45 mM⁻¹ cm⁻¹. Samples for thermal relaxation were prepared at 5 μ M final protein concentration in 1x TAE, 100 mM NaCl pH 7.5. The protein samples with non-specific DNA consisted of the same 5 μ M protein in 1 × TAE, 100 mM NaCl, pH 7.5 buffer but with sheared salmon testes DNA added to a final concentration of 1 mg/mL. Samples with target DNA contained in addition to the salmon testes DNA, an equimolar (*i.e.* 5 μ M) amount of annealed AP-1 DNA duplex. Irradiation of the protein sample was carried out by using a Luxeon III Star LED Royal Blue (455 nm) Lambertian operating at approximately 340 mW (700 mA). Relaxation rates at 20°C were measured by recording the change in absorbance at 350 nm. Data were fitted to single exponential functions to extract rate constants.

Urea Denaturation Studies

Protein samples ($\sim 5~\mu M$) were prepared in 1× TAE, 100 mM NaCl, pH 7.5 with 8M urea. Fluorescence emission at 360 nm (excitation at 280 nm, 2 nm excitation and emission slits) was monitored as the solution was titrated with the same solution without urea using an AVIV (Lakewood, NJ, USA) ATF-105 automatic titrating fluorometer. Data were recorded at 1 minute intervals with stirring upon each addition. Fluorescence refolding curves were obtained at 20°C and 30°C. Fluorescence data were then fitted using the equation:

$$F_{360nm} = \frac{(\alpha_N + \beta_N [\text{urea}]) + (\alpha_D + \beta_D [\text{urea}] \exp[m_{D-N} ([\text{urea}] - [D]^{50\%})/RT])}{1 + \exp[m_{D-N} ([\text{urea}] - [D]^{50\%})/RT]}$$
(1)

where α_N is $F_{360\text{nm}}$ in the absence of urea, β_N is the slope ($F_{360\text{nm}}$ vs. [urea]) at the beginning of the curve, α_D is the value of $F_{360\text{nm}}$ for the fully denatured state and β_D the slope at the end of the transition. The quantity 50% is the urea concentration at the point where the protein is 50% unfolded and the term $[D]^{50\%}$ is a proportionality constant that reflects the degree of unfolding of the protein in urea (13). Differential values for the free energies of folding of mutants versus GCN4 Δ 25PYP-v2 protein at the midpoint urea concentration were obtained from $\Delta\Delta G([D]^{50\%}) = 0.5(m_{D-N} + m'_{D-N}) \Delta([D]^{50\%})$ and for $\Delta\Delta G(H_2O) = m_{D-N}([D]^{50\%}) - m'_{D-N}([D]^{50\%})$ (14) where the term m'_{D-N} refers to the mutant.

DNA binding assays

All samples for electrophoretic mobility shift assay were prepared under red light. To 20 mM Tris.HCl, pH 7.5; 100 mM KCl, 3 mM MgCl₂, 0.1% Triton, 5% glycerol, 100 μ g/mL BSA, and 1 mg/mL sheared salmon testes DNA was added 10 nM annealed Cy-3 labelled AP-1 DNA and the GCN4 Δ 25PYP-v2 mutant protein at final concentrations of 1 nM, 5 nM, 10 nM, 25 nM, 50 nM, 75 nM, 100 nM, 125 nM, 250 nM, 375 nM, 500 nM, 750 nM, 1 μ M and 3 μ M in a total volume of 100 μ L. Samples were incubated overnight in the dark at 4°C or 20°C. The following day 20 μ L of the sample was run in the dark on an 8% native polyacrylamide gel containing 1× TAE, pH 7.5 buffer which is also used as the running buffer. Gels were run at 4°C for 105 minutes at 300 V using an Emperor Penguin Water cooled dual-gel electrophoresis system. The gel was scanned with a green laser (532 nm) on a GE Healthcare Typhoon 9400. The remaining samples were irradiated with a Luxeon III Star LED Royal Blue (455 nm) for 5 minutes and then another 20 μ L aliquot loaded on to another 8% native polyacryamide gel prepared as above. The gel was run and imaged as above except that two Luxeon III Star LED Royal Blue (455 nm) each at 340 mW (700mA)

were irradiating the gel continuously during the run. Heat from the LEDs was dissipated by the temperature-regulated gel tank buffer. To determine the reversibility of DNA binding, the remaining samples were incubated in the dark overnight and then a 20 μL aliquot run on another 8% native polyacryamide gel prepared as above. The gel was run in the dark and imaged as detailed above. DNA binding was quantified by analysis with ImageQuant 5.0 software. Using Igor Pro software, each set of data was fit to the Hill equation to determine apparent K_ds , the concentration of protein required for half-maximal binding to the AP-1 site, and Hill coefficients. Hill coefficients were found to vary between 1.6 and 2.6 when left unconstrained in the fitting. Hill coefficients were then constrained to 2 and apparent K_ds recalculated. The average and standard deviation from fits of experiments performed in triplicate are reported.

Results

Mutational design

In designing a GCN4 Δ 25PYP hybrid, our intent was to choose a GCN4 segment that could pack against the PYP core (residues 59–157) in the dark-adapted state in a manner that sterically impedes the ability of the coiled-coil domain to dimerize (8). When irradiated, this N-terminal cap region (residues 32–58) is anticipated to disengage from the PYP core and expose the coiled-coil sequence leading to dimerization and DNA binding. The amino acid sequence of GCN4 Δ 25PYP-v2 is shown in Scheme I.

To improve the degree of switching of DNA binding, our aim was to decrease affinity for DNA in the dark while maintaining or enhancing it in the light. It is useful to consider what classes of mutation might be expected. For instance, one could alter residues in GCN4Δ25PYP-v2 that comprise part of the basic DNA binding region (residues 8–23). Since this region is not expected to interact with the PYP domain in the light or the dark, mutations would be expected to affect light and dark GCN4Δ25PYP-v2 DNA affinity equally, *i.e.* have no effect on the degree of switching. Similarly, changes to residues that comprise part of the PYP core but that do not interact with the N-terminal cap would not be expected to alter DNA binding in the light or dark unless they substantially altered the overall light-driven conformational change. Therefore, we focused on residues that form part of the N-terminal cap (residues 32–58). These are expected to interact with the PYP core (residues 59–157) in the dark but interact with another N-terminal cap (to form a coiled-coil) when irradiated. In addition, residues in the PYP core domain that interact with the N-terminal cap in the dark may help to stabilize the dark state (and thereby decrease DNA binding affinity in the dark), but have no direct effect on the coiled coil structure.

Using the modeled structure of the PYP domain of GCN4 Δ 25PYP-v2 (8), which is based on the high resolution X-ray structure of wild-type PYP (PDB: 1NWZ) (15), we used the program PoPMuSiC 2.0 (http://babylone.ulb.ac.be/popmusic) to identify residues for which stability of the dark state protein might be enhanced. This program uses statistical potentials that combine four distinct protein sequence and structure descriptors and takes into account amino acid volume variation upon mutation. The calculated stability change also depends on the calculated solvent accessibility of the mutated residue. The key feature of PoPMuSiC 2.0, in addition to its superior performance in tests against experimental data, is that it is capable of rapidly predicting the stability changes resulting from all possible mutations in a protein (16,17). Using the PoPMuSiC 2.0 algorithm, sites predicted to be most likely to lead to enhanced protein stability were identified. These are collected in Table I together with the mutations that are predicted to be stabilizing.

Of these sites, E35, E45 and G54 are all part of the N-terminal cap while K143 and K144 are part of the PYP core domain that interacts with the N-terminal cap. In contrast, Q65 and R85 do not appear to interact with the N-terminal cap and were therefore excluded.

Any changes made to the N-terminal cap sequence must also be considered in terms of their potential effects on coiled coil formation – the intended light-adapted state. To assess effects of mutations on coiled-coil formation we used the algorithm for predicting coiled-coil stability developed by Arndt and colleagues (bCIPA,

http://www.molbiotech.uni-freiburg.de/bCIPA/). Coiled-coils are characterized by a heptad repeat sequence, *abcdefg*, where *a* and *d* positions form the hydrophobic dimerization interface and are particularly important for stability. In addition, the Asn residue that occurs at an *a* position in GCN4 (N16 in the wt sequence) is known to promote the formation of parallel, dimeric, coiled-coil structures and disfavor the formation of higher-ordered coils (18). Mutations at this position and at *a* and *d* sites were avoided. Table II lists all the options examined and their expected melting temperatures. The higher the melting temperature, the more stabilizing the mutation.

Residues identified as stabilizing by the PoPMuSiC 2.0 algorithm at position E35 include the hydrophobic residues F, L, I, W, Y, M, and V. Of these, none are stabilizing with respect to coiled coil formation; the least detrimental are L and M. At the E45 site, again PoPMuSiC 2.0 suggests hydrophobic residues (I, V, F, L, M, and Y). This site is an e position of the heptad and therefore can interact with the preceding g position of the other monomer in the coiled coil (Table II). Often in coiled coils such e-g' interactions are electrostatic in nature (20). However, in this case, a glycine residue was introduced in the preceding g position (8) since this residue in PYP adopts torsion angles only available to Gly in the Ramachandran plot and is partially conserved (21). While the Glu residue (the GCN4 Δ 25PYP-v2 residue) is the most stabilizing at position 45, a variety of other residues are compatible with coiled coil formation with relatively minor negative effects on stability (Table II). The PoPMuSiC 2.0 algorithm predicts that the G54 site may be mutated to A, E, D, or S with an increase in stability. The bCIPA algorithm predicts that any of these mutations but particularly G54E and G54A will also enhance coiled-coil stability.

The other two residues suggested by PoPMuSiC 2.0 as sites for enhancing stability were K143 and K144. These are sites that are part of the PYP core domain and so changes to either of these residues are not expected to affect coiled-coil stability in the light state. However both residues can interact with the N-terminal cap (32–58) with K143 making closer contact with the cap than K144. K143 is in close proximity to E45; in fact these residues make a salt bridge in the X-ray crystal structure (E12-K110 in wild type numbering) that has been proposed to be important for N-terminal cap stability (22). As a result, changes to residues E45, K143, and K144 are likely to be interdependent.

We explored interdependent mutations of the group of residues E35, E45, G54 K143 and K144 using the Rosetta design algorithm (23) as well as the Eris protein stability prediction server (http://troll.med.unc.edu/eris/login.php) (24,25). The Rosetta design algorithm was used previously in the design of GCN4 Δ 25PYP-v2 (8). Rather than using Rosetta for extensive redesign we focused on generating mutations at the E35, E45, G54 K143 and K144 sites to search for optimal combinations of changes. Rosetta predicted the largest stability improvement would occur with E35 changed to either A or M (E35A, E35M), G54 changed to E (G54E), E45 changed to K together with K143 changed to I (E45K-K143I) and K144 unchanged. The Eris server calculates the change of the protein stability induced by mutations utilizing the Medusa modeling suite. Whereas the Rosetta approach used a fixed backbone, the Eris server permits backbone flexibility. The Eris server returned E35A as preferable to E35M and G54E and G54A as equally stabilizing. Mutation to hydrophobic

residues was predicted to be particularly stabilizing at K143, more so than at K144. Additionally, if K143 was mutated to a hydrophobic residue, both the Eris server and the PoPMuSiC 2.0 algorithm indicated that further mutation of K144 to a hydrophobic residue would not lead to further stabilization. Since we also wanted to avoid the creation of hydrophobic patches on the protein surface that may lead to lower solubility and possible aggregation, we opted to focus hydrophobic mutation at position K143. The mutations ultimately chosen for mutation were thus: G54A, G54E, K143I, K143F, G54E-K143I, E35M-G54E-K143F, E45K-G54E-K143I, and E35M-E45K-G54E-K143I. These are highlighted in Table II, and Figures 1 and 2 in orange.

Protein expression, purification and preliminary characterization

Single point mutations in GCN4 Δ 25PYP-v2 were introduced using the Stratagene Quikchange protocol (Agilent, Inc.) and confirmed by automated DNA sequencing (ACGT Corp, Toronto). Each of the mutants was expressed in *E. coli* BL21cells; the 4-hydroxycinnamic acid chromophore, activated as a thioester (12), was added during expression. All mutants expressed well and were purified by immobilized metal affinity chromatography and analyzed by electrospray mass spectrometry. The masses observed were consistent with >95% holoprotein without any N-terminal processing. All proteins gave dark-adapted absorbance spectra similar to that of GCN4 Δ 25PYP-v2 (Fig. 3). The wavelengths of the absorbance maxima are all close to 446 nm \pm 2 nm, similar to wild type PYP (26). Absorbance ratios (A₄₄₆/A₂₈₀) were generally near 2.0 consistent with >95% holoprotein (26). Some variation in this ratio may be due to effects of mutations on absorbance coefficients. The presence of apoprotein would be expected to decrease the degree of photoswitching of DNA binding observed since apoprotein would bind DNA with the same affinity whether dark-adapted or irradiated.

Stability of the dark-adapted state: Urea denaturation

To assess the effects of mutation on the stability of dark-state GCN4 Δ 25PYP-v2 mutants, urea denaturation experiments were performed by measuring the fluorescence emission at 360 nm (excitation at 280 nm) as a function of urea concentration. A temperature of 30°C was used so that complete denaturation of the most stable mutants was observed. Similar relative stabilities among mutants were observed at 20°C. Figure 4 shows the urea denaturation curves measured for the mutants together with those for GCN4 Δ 25PYP-v2, wild type PYP, and for 25PYP. The denaturation midpoints together with estimated Δ Δ G's for folding (assuming a simple two-state model) (13) are collected in Table III. Clearly some of the designed mutations have indeed stabilized the dark adapted protein compared to GCN4 Δ 25PYP-v2. It appears that hydrophobic mutations at K143 are particularly effective as predicted by the PoPMuSiC 2.0 algorithm.

Effects of DNA addition: Thermal relaxation rates monitored using UV-Vis

To probe the interaction of the mutants with AP-1 DNA, the thermal relaxation of the constructs was measured by monitoring the decay of absorbance at 350 nm (pB form) as a function of time in the presence and absence of non-specific and specific (AP-1) DNA. These data are collected in Table IV. Rate constants derived from fitting to either a single exponential process or double-exponential processes were obtained. Lee and Hoff have suggested that double-exponential decays in PYP may arise from formation of a fraction of a cis proline isomer upon irradiation that subsequently reverts to a trans proline isomer (27). While fitting to double exponential decays did provide better fits to the data in some cases, single exponential fits also clearly reflected overall effects of DNA binding on thermal relaxation. At the protein and DNA concentrations tested, all the protein is expected to become DNA bound upon addition of AP-1 DNA whether the protein is irradiated or darkadapted (see below).

The deletion of the N-terminal cap has previously been shown to slow the PYP photocycle (28,29). Although, $\Delta 25$ PYP does not bind DNA specifically, addition of non-specific DNA slows the relaxation rate of $\Delta 25$ PYP somewhat perhaps via interactions with exposed hydrophobic surface of the protein. The relaxation rate of the pB form of GCN4 $\Delta 25$ PYP-v2, in contrast, is specifically slowed ~6-fold by binding to AP-1 DNA, whereas non-specific DNA causes a slight acceleration in the rate. The mutants show a variety of effects; in some cases (*e.g.* E45K-G54E-K143I) non specific DNA has a pronounced slowing effect, with subsequent specific binding to AP-1 having a less dramatic effect. In other cases (*e.g.* K143F, G54E-K143I), non specific DNA has a minimal effect and AP-1 DNA has a marked effect, slowing relaxation almost 10-fold.

Photo-switchable DNA binding activity

We further assayed the ability of the mutants to specifically recognize the AP-1 sequence by performing electrophoretic mobility shift assays using Cy3-labeled AP-1 in the presence of excess non-specific DNA. DNA binding affinities of the proteins in the dark-adapted state and irradiated state were calculated based on analysis of these gels and fitting to the Hill equation as described (8). Apparent affinities (the protein concentration required for half-maximal binding) are collected in Table V and sample data for the mutant showing the largest change in affinity upon irradiation (K143F) are shown in Figure 5. All binding was reversible.

The parent protein GCN4 Δ 25PYP-v2 shows an enhanced affinity for AP-1 when irradiated. The observed 2-fold decrease in apparent K_d (571 ± 17 to 297 ± 11 nM), while small, is reproducible and reversible after dark-adaptation. All of the mutants studied also showed enhanced DNA binding upon irradiation. In some cases (e.g. E45K-G54E-K143I) this was minimal, whereas in others (e.g. K143F, G54E-K143I) this was significantly enhanced compared to the parent. In addition the dark-adapted DNA binding affinity varied considerably. In some cases it was similar to or weaker than GCN4 Δ 25PYP-v2, but in many cases it was significantly tighter. In some (e.g. E45K-G54E-K143I) approaching that of free wild-type GCN4 without PYP (30)(apparent K_d ~ 60 nM). Hill coefficients derived from fitted binding curves varied between 1.6 and 2.6 suggesting the proteins dimerize upon binding to DNA as occurs for native GCN4 (30). Constraining the Hill coefficients to 2 gave apparent K_d values similar to those obtained using unconstrained fits. Forcing the Hill coefficient to be 1 gave very poor fits.

Further characterization of the K143F mutant

Since the GCN4 Δ 25PYP-v2-K143F mutant showed the largest effect of irradiation on specific AP-1 DNA binding as well as the largest increase in dark state stability, we characterized that mutant further to confirm its molecularity in the dark-adapted state in the absence of DNA as well as its DNA binding stoichiometry.

Size exclusion chromatography analysis confirmed that GCN4 Δ 25PYP-v2-K143F behaved as a monomer in the dark (Fig. 6A). Its elution volume matched that of GCN4 Δ 25PYP-v2 and was much larger than that of GCN4-PYP for which equilibrium analytical ultracentrifugation analysis yielded monomer and dimer masses respectively (8).

Measurement of the thermal relaxation rate of the pB form of the protein as a function of the concentration of AP-1 DNA (Fig. 6B) confirmed that GCN4 Δ 25PYP-v2-K143F bound DNA as a dimer. No further slowing of the relaxation rate was observed after a mole ratio of 1:2 (DNA: protein) was reached.

Discussion

Our intent in this work was to increase the degree of photoswitchable specific AP-1 DNA binding by the designed chimeric protein GCN4 Δ 25PYP-v2. Strickland *et al* have pointed out that fusion of a switchable protein to an intended effector domain is likely to alter the on-off balance of the switchable domain (7). In the case of the LOV photoswitchable domain fused to the Trp repressor, packing of the *J*-alpha helix against the LOV domain is intended in the dark. In their original design, fusion to the Trp repressor appears to destabilize the packing of the helix so that when the LOV domain is irradiated, only a small extra degree of disengagement of the *J*-alpha helix is possible, hence the degree of photo switching is small. By stabilizing the helix packing against the LOV domain in the dark state of the chimera with a few carefully chosen mutations, these authors were able to increase the degree of photo switching substantially (7).

In the present case, we were seeking to pack the dimerizing coiled-coil domain of GCN4 against the PYP core in the dark thereby diminishing its DNA binding ability. At the same time, we wished to preserve high affinity specific DNA binding in the irradiated state. As a framework for considering the results obtained it is useful to view the system as the thermodynamic cycle shown in Figure 7. Four states are identified: (i) a folded PYP domain (pG) with the GCN4 zipper domain packed against the PYP core, (ii) a folded PYP domain (pG) with the GCN4 zipper domain dimerized and bound to DNA, (iii) a partially unfolded PYP domain (pB) with the GCN4 zipper domain dimerized and bound to DNA, and (iv) a partially unfolded PYP domain (pB) with the GCN4 zipper domain free. Shining blue light on the system may be regarded as perturbing it in a manner that produces pB states (iii, iv) at the expense of pG states (i, ii). In the dark these four states are connected in a thermodynamic cycle (Fig. 7) where:

$$K_{d app} light * K_{fold} = K_{d app} dark * K_{foldDNA}$$
 (2)

As in the LOV/Trp repressor case, we anticipated that introducing mutations that would stabilize the packing of the N-cap upon the PYP core would enhance photoswitching, if they would selectively stabilize state (i) and have no effect on states (ii)-(iv). Our approach to choosing the mutations was described in detail above. The mutations ultimately chosen were: G54A, G54E, K143I, K143F, G54E-K143I, E35M-G54E-K143I, E35M-G54E-K143F, E45K-G54E-K143I, and E35M-E45K-G54E-K143I. These sites are highlighted in Table II, and Figures 1, 2 and 7 in orange. All mutant proteins were expressed and purified, gave UV-Vis spectra like the parent protein GCN4 Δ 25PYP-v2, and underwent normal photocycles.

Urea denaturation studies were first performed to gauge the effects of mutations on dark state stability of the proteins. Whereas wild type PYP has a urea denaturation midpoint ([D]^{50%}) of 7.2 M (31), 25PYP, the protein missing the N-terminal cap entirely, has [D]^{50%} of 5.9 M (Table III). This result indicates that substantial stabilization is available from an N-terminal cap that is well packed onto the PYP core. The parent hybrid protein GCN4 Δ 25PYP-v2 has a urea midpoint slightly less than that of Δ 25PYP indicating that the N-terminal cap in that case contributes nothing to protein stabilization. Although CD and fluorescence data indicate the cap is packed against the core in GCN4 Δ 25PYP-v2 (8), it may be only loosely packed so that no overall stabilization is obtained.

Changes at position K143 to hydrophobic residues were predicted by PoPMuSiC 2.0 to be particularly stabilizing (Table I). Experimentally we found this to be the case. Both K143I and K143F mutations were significantly stabilizing. The K143F mutation increased the

 $[D]^{50\%}$ value to 6.9 M which corresponds an increase in stability of ~2.2 kcal/mol relative to GCN4 Δ 25PYP-v2 (14). Mutations at sites E35 and E45 that are part of the coiled-coil forming segment produced only small enhancements of stability. In contrast, G54A and G54E mutants proved to have almost no effect on stability.

The DNA binding abilities of these mutants were analyzed using electrophoretic mobility shift assays. There was no clear relationship between dark-sate stability as judged by urea denaturation experiments and specific AP-1 DNA affinity in the dark-adapted state. Whereas, the K143I and K143F mutations are both significantly more stable than GCN4 Δ 25PYP-v2, K143I has decreased dark-state AP-1 DNA binding affinity, while that of K143F was enhanced. The E35M-G54E-K143F and E45K-G54E-K143I mutants had enhanced stability and also enhanced dark-state DNA binding affinity.

When the proteins were irradiated, DNA binding affinity was enhanced in all cases consistent with enhanced exposure of the coiled-coil forming residues created by light driven detachment of the N-cap from the PYP core. However, rather than being silent in terms of light-state AP-1 DNA binding affinity, the set of mutations has a variety of effects, both weakening it (G54A, G54E) and enhancing it (*e.g.* K143F, E35M-G54E-K143F).

The thermodynamic cycle diagrammed in Fig 7 requires that, however the mutations are affecting the stability of states (i)-(iv), there should be a relationship between the degree of photoswitching (K_d app dark/ K_d app light) and the equilibrium constant for folding in the presence and absence of DNA (Eq. 2). In the dark, the pG (folded) state is substantially more stable than the pB state so that, at equilibrium, only the pG state is observed, making direct determination of K_{fold} and K_{fold} DNA difficult. However, we measured the folding rate (Table IV), *i.e.* the rate of the thermal pB to pG transition in the PYP photocycle, in the presence or absence of DNA (*i.e.* k_{fold} and k_{fold} DNA in Fig. 7). As noted above, at the protein and DNA concentrations employed for UV-Vis absorbance measurements the protein will be completely bound to AP-1 DNA in both the dark-adapted and irradiated state.

Although only the ratio of the equilibrium constants for folding, not the rate constants, are constrained by the thermodynamic cycle, there appears to be an approximately linear relationship between the ratio of these rate constants (Table IV) and the degree of photoswitching (Table V) as shown in Figure 8. In general, those mutants with a larger degree of photoswitching also have a slower refolding rate in the presence of DNA. That this relationship exists implies that the mutations are not substantially affecting the relative unfolding rates (k_{unfold} vs. k_{unfold} DNA).

Overall these results indicate that, given a well-defined folded structure, computational tools, particularly PoPMuSiC 2.0, can rapidly identify sites such as position 143 where mutations can have significant stabilizing effects. However, our assumption that a more stable dark-state structure would lead to a greater degree of photoswitching was clearly too simplistic. First, it may be that the stabilization of the dark-state, as judged by urea denaturation assays, does not directly reflect better packing of the N-cap domain on the PYP core, instead resistance to denaturation is perhaps achieved by other means. Alternatively, or in addition, it may be that the mutations are affecting the stability of states other than state (i) in Figure 7. This conclusion is supported by the finding that mutations are affecting refolding rates ($k_{\rm fold}$ and $k_{\rm fold}$ DNA), a result that would not be expected if only changes in the stability of state (i) were involved. Structural studies aimed at elucidating features of states (ii)—(iv) may therefore help guide further improvements in photoswitch design.

The mutant K143F that showed the largest degree of photoswitching (Table V, Fig. 5) with an almost 4-fold decrease in apparent K_d for AP-1 binding upon irradiation, also (together with G54E, K143I) was the mutant for which AP-1 DNA binding had the largest effect on

the photocycle kinetics (Fig. 8). The K143F mutant was also the most stable as judged by the urea denaturation assay ((Table III, Fig. 4). Further analysis of the GCN4 Δ 25PYP-v2 mutant by size exclusion chromatography showed that it behaved as a monomer in the dark (Fig. 6A). The relaxation rate of the pB state was found to slow as the concentration of AP-1 DNA increased until a mole ratio of one AP-1 DNA duplex to two GCN4 Δ 25PYP-v2-K143F proteins was reached (Fig. 6B). This result confirms that GCN4 Δ 25PYP-v2-K143F binds its target as a dimer, as designed. Overall the K143F mutant seems well behaved and a distinct improvement over the parent GCN4 Δ 25PYP-v2.

Although larger changes in DNA affinity are desirable before GCN4Δ25PYP proteins may be used as robust tools for photocontrol of transcription, if the K143F switchable protein were expressed at an ideal concentration, a ~12 fold-change in fraction DNA bound is possible due to the cooperativity of DNA binding by coiled coil proteins (the Hill coefficients for all mutants were near 2.0). Figure 9 shows binding curves for K143F with the observed apparent K_d (i.e. half maximal binding is 110 nM in the light and 380 nM in the dark). For simplicity we assume the full range (0-100%) of binding occurs whereas experimentally a maximum of ~90% fraction bound DNA is observed likely because of a small fraction of DNA is misfolded. Irradiation causes a decrease in apparent K_d and so an increase in fraction bound DNA for a given concentration of protein. The increase is plotted as a ratio (fraction bound DNA when irradiated / fraction bound DNA dark-adapted) as a function of protein concentration. The greatest increase in fraction bound DNA occurs at lower protein concentrations. For instance, at 40 nM K143F irradiation would cause an increase in fraction bound DNA from 1% to 12% (12-fold). If there were no cooperativity, the maximal increase would be only 3.5 fold (Fig. 9B). If further mutagenesis of GCN4Δ25PYP were to produce a protein that exhibited a 10-fold difference in the apparent K_d between dark and irradiated states (e.g. the apparent K_d of the dark-adapted protein was 1100 nM), a 100-fold change in fraction bound DNA would be possible (Fig. 9A). Note also that increasing the difference in apparent K_d between dark and irradiated states leads to a wider range of protein concentrations over which substantial increases in fraction DNA bound occur upon irradiation. Thus, photoswitch design should focus on maximizing the free energy difference between the dark and light states and then suitably poising the system in the dark state.

Changes in fractional occupancy of a regulatory binding site may be expected to lead to changes in gene expression levels. Changes of only 2- or 3-fold in gene expression level are sometimes associated with clear differences in phenotype (32–34) so that genetically encoded photochemical tools that would permit 10-100-fold changes in gene expression associated with AP-1 regulatory sites could be of substantial use, particularly for studies on the role of AP-1 dependent gene expression in cell proliferation, tumorogenesis, differentiation and apoptosis (35–37).

Acknowledgments

We wish to thank the Natural Sciences and Engineering Research Council of Canada, the Canadian Institutes of Health Research and the National Institutes of Health (U.S.A)(R01 MH086379) for financial support.

Abbreviations

PYP photoactive yellow protein

bZIP basic leucine zipper

PCR polymerase chain reaction

SDS-PAGE sodium dodecyl sulfate – polyacrylamide gel electrophoresis

ESI-MS electrospray ionization mass spectrometry

EDTA ethylenediamine tetraacetic acid

References

1. Deiters A. Light activation as a method of regulating and studying gene expression. Curr Opin Chem Biol. 2009; 13:678–686. [PubMed: 19857985]

- 2. Liu Y, He Q, Cheng P. Photoreception in Neurospora: a tale of two White Collar proteins. Cell Mol Life Sci. 2003; 60:2131–2138. [PubMed: 14618260]
- 3. Takahashi F, Yamagata D, Ishikawa M, Fukamatsu Y, Ogura Y, Kasahara M, Kiyosue T, Kikuyama M, Wada M, Kataoka H. AUREOCHROME, a photoreceptor required for photomorphogenesis in stramenopiles. Proc Natl Acad Sci USA. 2007; 104:19625–19630. [PubMed: 18003911]
- 4. Shimizu-Sato S, Huq E, Tepperman JM, Quail PH. A light-switchable gene promoter system. Nat Biotechnol. 2002; 20:1041–1044. [PubMed: 12219076]
- 5. Yazawa M, Sadaghiani AM, Hsueh B, Dolmetsch RE. Induction of protein-protein interactions in live cells using light. Nat Biotechnol. 2009; 27:941–945. [PubMed: 19801976]
- Strickland D, Moffat K, Sosnick TR. Light-activated DNA binding in a designed allosteric protein. Proc Natl Acad Sci USA. 2008; 105:10709–10714. [PubMed: 18667691]
- Strickland D, Yao X, Gawlak G, Rosen MK, Gardner KH, Sosnick TR. Rationally improving LOV domain-based photoswitches. Nat Methods. 2010
- 8. Morgan SA, Al-Abdul-Wahid S, Woolley GA. Structure-based design of a photocontrolled DNA binding protein. J Mol Biol. 2010; 399:94–112. [PubMed: 20363227]
- 9. Yin S, Ding F, Dokholyan NV. Computational evaluation of protein stability change upon mutations. Methods Mol Biol. 2010; 634:189–201. [PubMed: 20676985]
- Das R, Baker D. Macromolecular modeling with rosetta. Annu Rev Biochem. 2008; 77:363–382.
 [PubMed: 18410248]
- 11. Devanathan S, Genick UK, Getzoff ED, Meyer TE, Cusanovich MA, Tollin G. Preparation and properties of a 3,4-dihydroxycinnamic acid chromophore variant of the photoactive yellow protein. Arch Biochem Biophys. 1997; 340:83–89. [PubMed: 9126280]
- 12. Changenet-Barret P, Espagne A, Charier S, Baudin JB, Jullien L, Plaza P, Hellingwerf KJ, Martin MM. Early molecular events in the photoactive yellow protein: role of the chromophore photophysics. Photochem Photobiol Sci. 2004; 3:823–829. [PubMed: 15295641]
- 13. Fersht, A. Structure and mechanism in protein science. W.H. Freeman; New York: 1999.
- Clarke J, Fersht AR. Engineered disulfide bonds as probes of the folding pathway of barnase: increasing the stability of proteins against the rate of denaturation. Biochemistry. 1993; 32:4322–4329. [PubMed: 8476861]
- Getzoff ED, Gutwin KN, Genick UK. Anticipatory active-site motions and chromophore distortion prime photoreceptor PYP for light activation. Nat Struct Biol. 2003; 10:663–668. [PubMed: 12872160]
- 16. Dehouck Y, Grosfils A, Folch B, Gilis D, Bogaerts P, Rooman M. Fast and accurate predictions of protein stability changes upon mutations using statistical potentials and neural networks: PoPMuSiC-2.0. Bioinformatics. 2009; 25:2537–2543. [PubMed: 19654118]
- 17. Gilis D, Rooman M. PoPMuSiC, an algorithm for predicting protein mutant stability changes: application to prion proteins. Protein Eng. 2000; 13:849–856. [PubMed: 11239084]
- 18. Gonzalez L Jr, Woolfson DN, Alber T. Buried polar residues and structural specificity in the GCN4 leucine zipper. Nat Struct Biol. 1996; 3:1011–1018. [PubMed: 8946854]
- 19. Ellenberger TE, Brandl CJ, Struhl K, Harrison SC. The GCN4 basic region leucine zipper binds DNA as a dimer of uninterrupted alpha helices: crystal structure of the protein-DNA complex. Cell. 1992; 71:1223–1237. [PubMed: 1473154]

 Mason JM, Arndt KM. Coiled coil domains: stability, specificity, and biological implications. Chembiochem. 2004; 5:170–176. [PubMed: 14760737]

- 21. Imamoto Y, Tatsumi S, Harigai M, Yamazaki Y, Kamikubo H, Kataoka M. Diverse roles of glycine residues conserved in photoactive yellow proteins. Biophys J. 2008; 94:3620–3628. [PubMed: 18227128]
- 22. Hoersch D, Otto H, Joshi CP, Borucki B, Cusanovich MA, Heyn MP. Role of a conserved salt bridge between the PAS core and the N-terminal domain in the activation of the photoreceptor photoactive yellow protein. Biophys J. 2007; 93:1687–1699. [PubMed: 17496031]
- 23. Dantas G, Kuhlman B, Callender D, Wong M, Baker D. A large scale test of computational protein design: folding and stability of nine completely redesigned globular proteins. J Mol Biol. 2003; 332:449–460. [PubMed: 12948494]
- 24. Yin S, Ding F, Dokholyan NV. Eris: an automated estimator of protein stability. Nat Methods. 2007; 4:466–467. [PubMed: 17538626]
- 25. Yin S, Ding F, Dokholyan NV. Modeling backbone flexibility improves protein stability estimation. Structure. 2007; 15:1567–1576. [PubMed: 18073107]
- Philip AF, Eisenman KT, Papadantonakis GA, Hoff WD. Functional tuning of photoactive yellow protein by active site residue 46. Biochemistry. 2008; 47:13800–13810. [PubMed: 19102703]
- Lee BC, Hoff WD. Proline 54 trans-cis isomerization is responsible for the kinetic partitioning at the last-step photocycle of photoactive yellow protein. Protein Sci. 2008; 17:2101–2110. [PubMed: 18794212]
- 28. Harigai M, Yasuda S, Imamoto Y, Yoshihara K, Tokunaga F, Kataoka M. Amino acids in the N-terminal region regulate the photocycle of photoactive yellow protein. J Biochem. 2001; 130:51–56. [PubMed: 11432779]
- 29. Bernard C, Houben K, Derix NM, Marks D, van der Horst MA, Hellingwerf KJ, Boelens R, Kaptein R, van Nuland NA. The solution structure of a transient photoreceptor intermediate: Delta25 photoactive yellow protein. Structure. 2005; 13:953–962. [PubMed: 16004868]
- 30. Woolley GA, Jaikaran AS, Berezovski M, Calarco JP, Krylov SN, Smart OS, Kumita JR. Reversible photocontrol of DNA binding by a designed GCN4-bZIP protein. Biochemistry. 2006; 45:6075–6084. [PubMed: 16681380]
- 31. Meyer TE, Yakali E, Cusanovich MA, Tollin G. Properties of a water-soluble, yellow protein isolated from a halophilic phototrophic bacterium that has photochemical activity analogous to sensory rhodopsin. Biochemistry. 1987; 26:418–423. [PubMed: 3828315]
- 32. Antony AK, Kong W, Lorenz HP. Upregulation of neurodevelopmental genes during scarless healing. Ann Plast Surg. 2010; 64:247–250. [PubMed: 20098115]
- 33. Jais PH. How frequent is altered gene expression among susceptibility genes to human complex disorders? Genet Med. 2005; 7:83–96. [PubMed: 15714075]
- 34. Samaco RC, Fryer JD, Ren J, Fyffe S, Chao HT, Sun Y, Greer JJ, Zoghbi HY, Neul JL. A partial loss of function allele of methyl-CpG-binding protein 2 predicts a human neurodevelopmental syndrome. Hum Mol Genet. 2008; 17:1718–1727. [PubMed: 18321864]
- 35. Lopez-Bergami P, Lau E, Ronai Z. Emerging roles of ATF2 and the dynamic AP1 network in cancer. Nat Rev Cancer. 2010; 10:65–76. [PubMed: 20029425]
- 36. Wagner EF. Functions of AP1 (Fos/Jun) in bone development. Ann Rheum Dis. 2002; 61(Suppl 2):ii40–42. [PubMed: 12379619]
- 37. Karin M, Gallagher E. From JNK to pay dirt: jun kinases, their biochemistry, physiology and clinical importance. IUBMB Life. 2005; 57:283–295. [PubMed: 16036612]

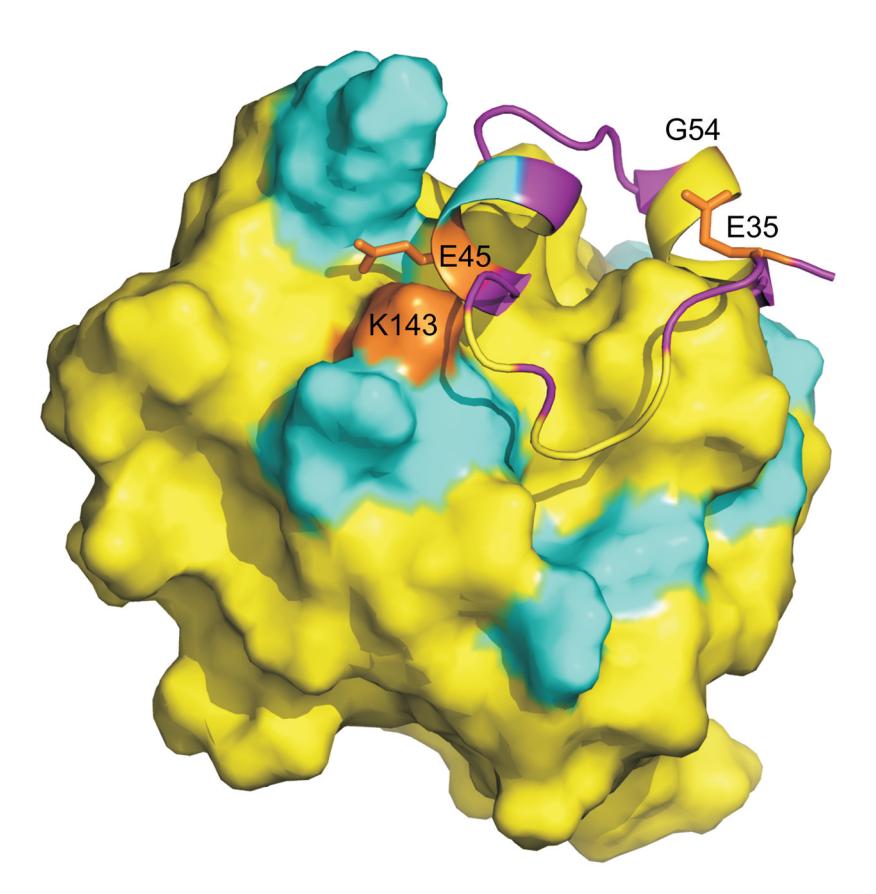


Figure 1. The sequence of GCN4 Δ 25PYP-v2 modeled onto the structure of wt-PYP (PDB: 1NWZ) (15). Residues 59–157 (the "core" domain) of PYP are shown as a solid surface. Residues that are part of GCN4 or the N-terminal cap (32–58) are shown as a ribbon. Colors follow the convention of Scheme I (PYP residues yellow, GCN4 residues purple, residues changed in the hybrid that are not PYP or GCN4 residues are cyan). The unstructured basic region sequence of GCN4 is truncated for clarity. Residues targeted for mutagenesis in the present study are colored orange and labeled.

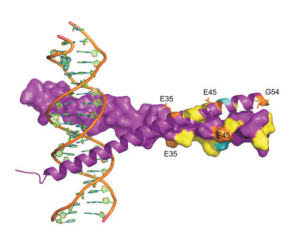


Figure 2.

The sequence of GCN4 Δ 25PYP-v2 modeled onto the structure of wt-GCN4 bound to DNA as a dimer (PDB: 1YSA) (19), the intended light-adapted state. Residues 59–157 of the PYP domain are omitted for clarity. One monomer is shown as a ribbon and the other as a solid surface. Colors follow the conventions of Scheme I (PYP residues yellow, GCN4 residues purple, residues changed in the hybrid that are not PYP or GCN4 residues are cyan). Residues targeted for mutagenesis in the present study are colored orange and labeled.

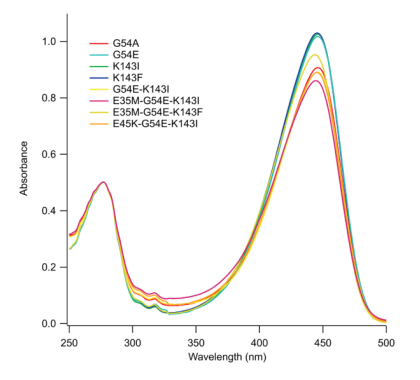


Figure 3. UV-Vis spectra of a subset of GCN4 Δ 25PYP-v2 mutants in TAE, pH 7.5, 100 mM NaCl at 4°C. Protein concentrations were approximately 5 μ M (absorbance was normalized at 278 nm).

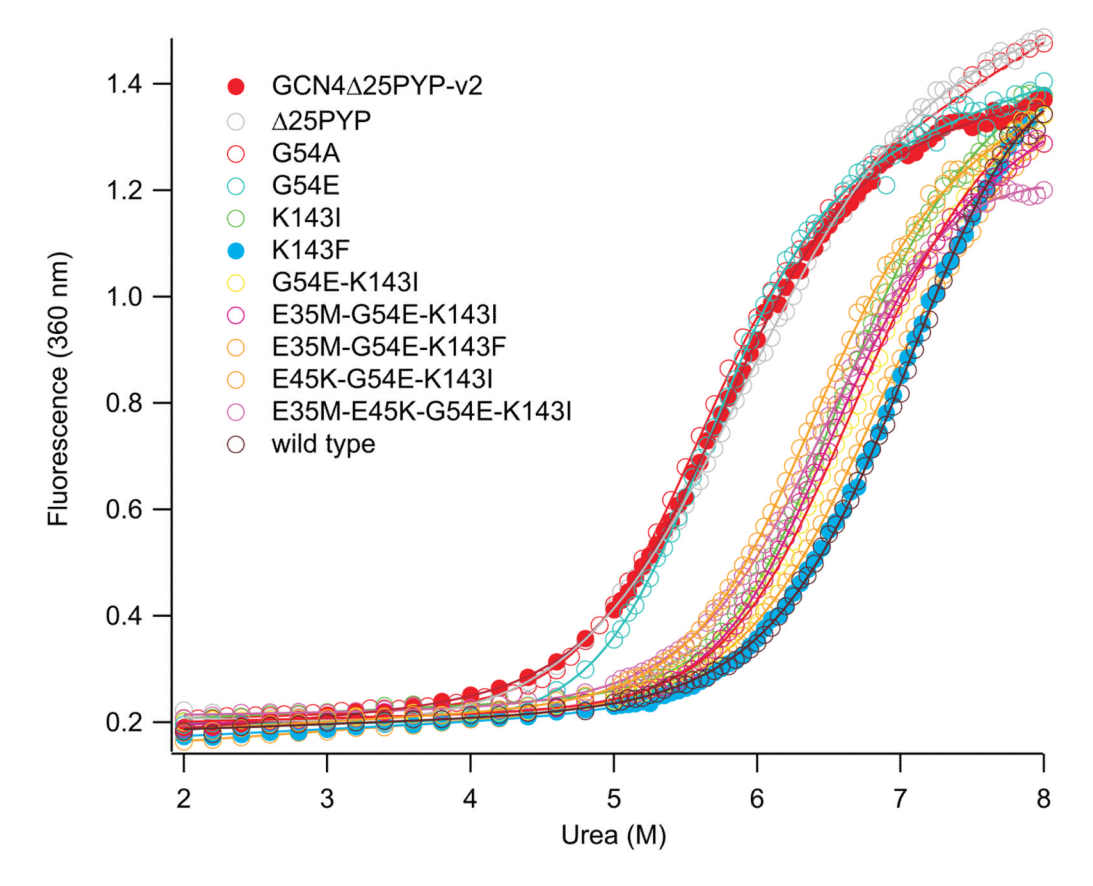


Figure 4. Urea denaturation of GCN4 Δ 25PYP-v2 mutants in TAE, pH 7.5, 100 mM NaCl at 30°C as monitored by measuring fluorescence emission at 360 nm (excitation at 280 nm). Protein concentrations were approximately 5 μ M.

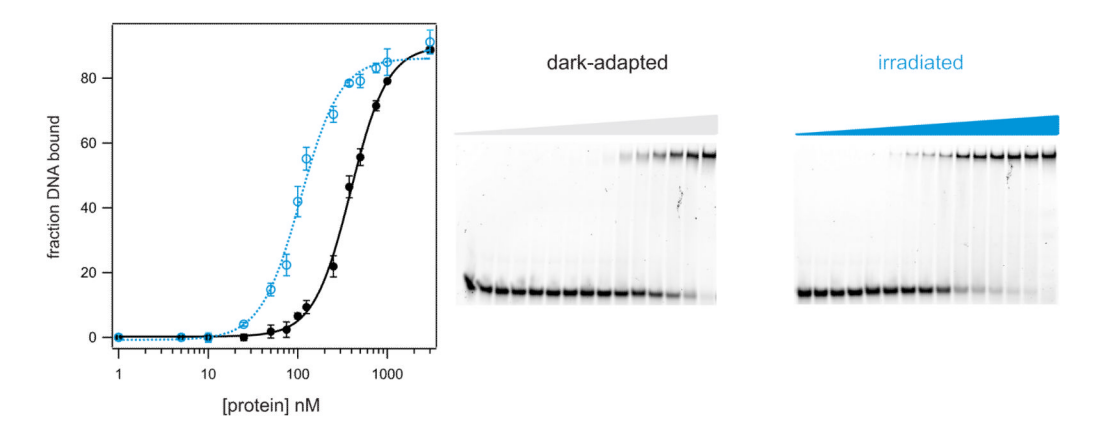


Figure 5. EMSA of the GCN4 Δ 25PYP-v2-K143F mutant with AP-1 target DNA. Binding buffer was 20 mM Tris pH 7.5, 100 mM KCl, 3 mM MgCl₂, 0.1% Triton, 5% glycerol 100 µg/mL BSA, 1 mg/mL salmon testes DNA. 5'-Cy-3 labelled AP-1 DNA, 10 nM. Running buffer was TAE buffer pH 7.5. Gels were run either in the dark or under constant 460 nm LED illumination at 4°C. Protein concentrations on gel images shown were: 0, 1, 5,10, 25, 50, 75, 100, 125, 250, 375, 500, 750, 1000, 3000 nM.

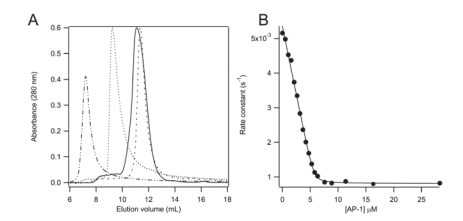


Figure 6.
(A) Size-exclusion (G75) chromatography of dark-adapted GCN4Δ25PYP-v2-K143F (—) in TAE buffer pH 7.5, 100 mM NaCl. GCN4PYP (- - -) is dimeric (44790 Da) and GCN4Δ25PYP-v2 (- - -) is monomeric (19644 Da) under these conditions ((8)). The elution pattern of blue dextran (- . . -) indicates the void volume of the column. (B) Rate constants calculated from exponential fits to pB thermal relaxation data (absorbance at 350 nm) for 10 μM GCN4Δ25PYP-v2-K143F in the absence of AP-1 DNA and with increasing amounts of AP-1 DNA in TAE buffer pH 7.5, 100 mM NaCl, 20°C, plus 1 mg/ml salmon testes DNA.

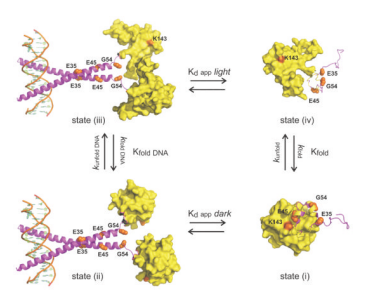


Figure 7.

A thermodynamic cycle describing DNA binding by GCN4 Δ 25PYP fusion proteins. All structures are models only. Coloring is the same as in Figures 1 and 2 except cyan colors are omitted for clarity. GCN4 residues are purple and PYP residues are yellow. Mutated sites are shown in orange spacefill. Surfaces represent the core of PYP (residues 59–157). State (i) is the folded dark state structure based on wild type PYP (PDB code 1NWZ). State (ii) retains the dark state fold of the PYP core but the N-cap residues are unpacked from the PYP core and participate in coiled-coil formation. The coiled coil is based on wild type bZIP GCN4 bound to DNA (PDB code 1YSA) (19). State (iii) is the same as state (ii) except that the PYP core is partially unfolded. One structure from the NMR derived ensemble of structure for light adapted Δ 25 PYP is shown (PDB code 1XFQ) (29). State (iv) is the partially unfolded core of PYP with the N-cap detached.

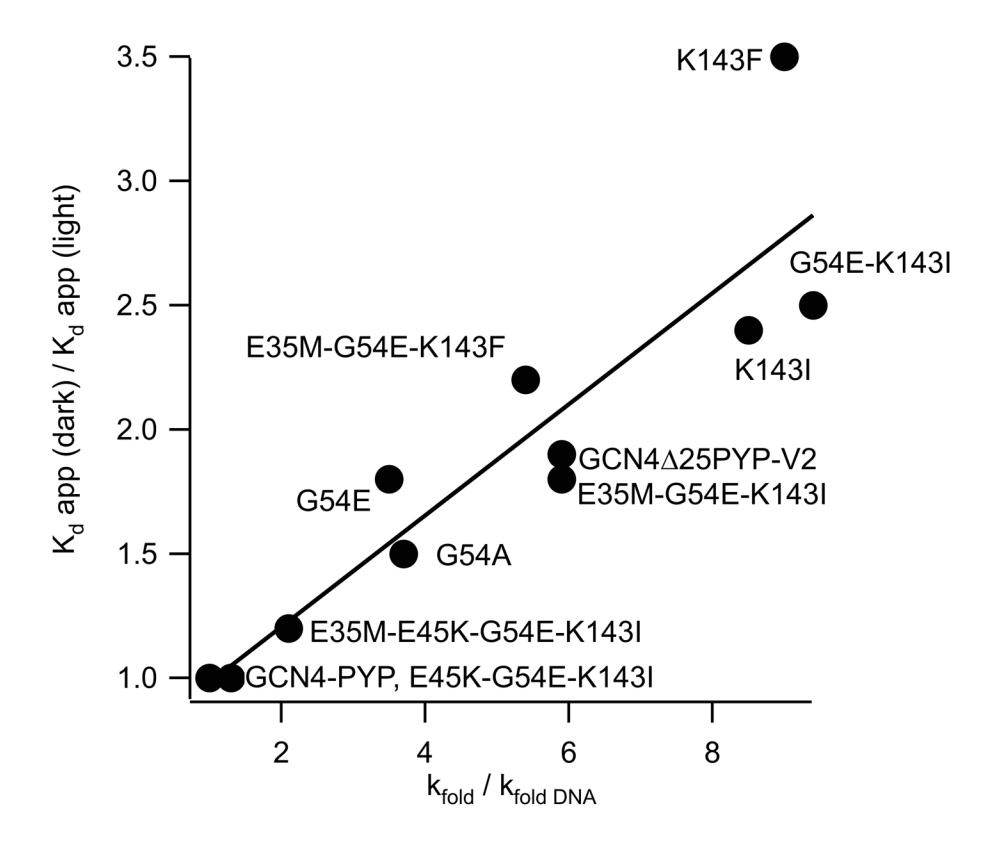


Figure 8. Observed relationship between the degree of photoswitching of AP-1 DNA binding (K_d app dark/ K_d app light) and the ratio of k_{fold} and k_{fold} DNA (see Fig. 7).

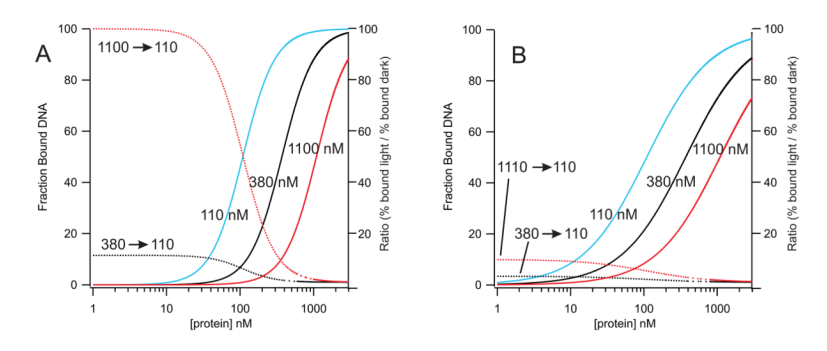


Figure 9. Calculated percentage bound DNA (solid curves, left hand ordinate) assuming (A) cooperative binding (Hill coefficient = 2) (B) non-cooperative binding. Apparent K_{dS} are 110 nM (blue), 380 nM (black), and 1100 nM (red). Dotted curves are the calculated ratio of % bound DNA in the light / % bound DNA in the dark. Dotted curves use the right hand ordinate.

8 23 32
MKDPAALKRARNTEAARRSRARKLQRMKQLEDKVEELAFGNEHLEEELARLKKGQLDRLAFGAIQLDGDGNILQY
NQQEGDITGRDPSQVIGKNFFKDVAPCTDSPEFYGKFKEGVASGNLQTMFEYTFDYQMTPTKVRVFMKKSKTGD
SYWVFVTRVKLAAALEHHHHHH

Scheme I.

Primary sequence of the GCN4 Δ 25PYP-v2 protein (purple-gcn4 residue; yellow-pyp residue; cyan- residue chosen by Rosetta, red-vector encoded His tag)(32–58: N-terminal cap)

Table 1

Sites and mutations predicted to enhance GCN4 Δ 25PYP-v2 stability by PoPMuSiC 2.0. Numbers in brackets are the calculated difference in dark state (pG) folded stability in kcal/mol.

Residue in GCN4Δ25PYP-v2	Stabilizing mutations
E35	F (-1.60), L (-1.54), I (-1.52), W(-1.34), Y(-1.30), M(-1.21), V(-1.10), H(-0.61), Q(-0.29), R(-0.20), T(-0.33)
E45	I (-0.71), V (-0.43), F(-0.41), L(-0.35), M(-0.32), Y(-0.21)
G54	A(-0.44), E(-0.36), D(-0.32), S(-0.30)
Q65	I(-0.86), L(-0.50), V(-0.46), M(-0.46), F(-0.44), W(-0.42), Y(0.40), H(-0.30)
R85	I(-0.60), L(-0.58), W(-0.40), Y(-0.37), V(-0.30), M(-0.27), F(-0.22)
K143	F(-1.02),L(-0.76),Y,(-0.66),I(-0.64),W(-0.64),V(-0.59),M(-0.44),H(-0.14)
K144	L(-0.72), $W(-0.63)$, $F(-0.51)$, $M(-0.46)$, $I(-0.45)$, $Y(-0.36)$, $V(-0.27)$, $P(-0.11)$

Table 2

Calculated stabilities of single point mutants of the coiled-coil forming domain of GCN4 Δ 25PYP-v2. Heptad positions that can make electrostatic interactions (g,e) are indicated with the same color. Only a limited number of mutations were considered at a and d (core hydrophobic) positions. Proline and cysteine substitutions were not considered.

GCN4Δ25PYP-v2 numbering	27 28	29 3	31	32 33	34	35	36	37	38	39	40	41	42	43	44	45	46	47	48	49	50	51	52	53	54	55	56	57	58
heptad position	a b	c d	е	f g	а	b	С	d	e	f	g	а	b	С	d	е	f	g	а	b	С	d	e	f	g	а	b	С	d
GCN4Δ25PYP-v2 sequence	M K	Q L	Ε	D K	٧	E	Е	L	Α	F	G	N	Е	Н	L	Ε	Е	E	L	Α	R	L	K	K	G	Q	L	D	R
A					26	24	24		27	30	38	28	24	31		24	24	12		27	29		16	29	38	34	27	32	3.5
D					15	19	19		26	25	25	18	19	26		19	19	11		22	24		2	24	33	23	22	27	2
E					22	27	27		42	32	32	25	27	33		27	27	27		29	31		9	31	40	30	30	34	3:
F					17	21	21		24	27	35	20	21	28		21	21	9		24	26		13	26	35	25	24	29	2
G					8	13	13		15	18	27	11	13	19		13	13	0		15	17		4	17	27	17	16	20	1
н					16	20	20		22	25	34	18	20	27		20	20	7		22	25		12	24	34	24	23	27	2
I					28	21	21		23	26	34	31	21	27	18	21	21	8		23	25		12	25	34	36	24	28	3
K					18	22	22		16	27	49	20	22	29		22	22	1		24	27		27	27	36	26	25	29	2
L					37	24	24	27	26	29	37	39	24	30	27	24	24	11	27	26	28	27	15	28	37	45	27	31	46
М					19	23	23		25	28	37	21	23	30		23	23	10		25	28	8	15	27	37	27	26	30	2
N					24	17	17		19	22	31	27	17	23		17	17	4		19	21		8	21	31	32	20	24	3
Q					18	23	23		34	28	41	21	23	29		23	23	19		25	27		18	27	37	27	26	30	2
R					18	22	22		16	27	49	20	22	28		22	22	1		24	27		26	26	36	26	25	29	2
S					10	14	14		17	20	28	13	14	21		14	14	2		17	19		6	19	28	18	17	22	19
T					12	17	17		19	22	31	15	17	23		17	17	4		19	21		8	21	31	21	20	24	2
V					27	19	19	16	21	24	33	29	19	26		19	19	6	16	21	24		11	24	33	35	22	26	36
W					15	20	20		22	25	34	18	20	26		20	20	7		22	24		11	24	34	24	23	27	2
Υ					12	17	17		19	22	30	15	17	23		17	17	4		19	21		8	21	30	20	19	24	2
wt gcn4 numbering	2 3	4	5 6	7 8	9	10	11	12	13	14	15	16	17	18	19	20	21	22	23	24	25	26	27	28	29	30	31	32	3:
wt PYP numbering					1	2	3	4	5	6	7	8	9	10	11	12	13	14	15	16	17	18	19	20	21	22	23	24	2
XX most stabilizing mutation	gc	n4 res	idue		PYF	res	idue	è			mu	tatio	on ta	arge	t			Ros	etta	mu	tati	on							

Table 3

Calculated midpoints ([D]^{50%}) for urea denaturation of GCN4 Δ 25PYP-v2 mutants in TAE, pH 7.5, 100 mM NaCl at 30°C. Values for $m_{\text{D-N}}$ and free energies ($\Delta\Delta G([D]^{50\%})$, ($\Delta\Delta G(H_2O)$) were estimated as described in the Methods section.

Protein	[D] ^{50%} Molar	m _{D-N} kcal/mol ²	$\Delta\Delta G([\mathrm{D}]^{50\%})$ kcal/mol	ΔΔG(H ₂ O)kcal/mol
GCN4Δ25PYP-v2	5.72 ± 0.01	1.29 ± 0.03	-	-
Δ25ΡΥΡ	5.84 ± 0.03	0.99 ± 0.02	-0.20	1.6
G54A	5.46 ± 0.01	1.45 ± 0.04	0.54	-0.5
G54E	5.61 ± 0.02	1.51 ± 0.03	0.24	-1.1
K143I	6.43 ± 0.02	1.52 ± 0.03	-1.54	-2.4
K143F	6.88 ± 0.05	1.22 ± 0.02	-2.16	-1.0
G54E-K143I	6.53 ± 0.03	1.34 ± 0.03	-1.61	-1.4
E35M-G54E-K143I	6.40 ± 0.03	1.49 ± 0.04	-1.45	-2.1
E35M-G54E-K143F	6.71 ± 0.03	1.27 ± 0.02	-1.90	-1.1
E45K-G54E-K143I	6.30 ± 0.03	1.41 ± 0.04	-1.19	-1.5
E35M-E45K-G54E-K143I	6.53 ± 0.03	1.26 ± 0.03	-1.54	-0.9
Wild-type	7.20 ± 0.08	1.21 ± 0.03	-2.75	-1.3

 $\label{eq:Table 4} \textbf{Lifetimes for thermal relaxation of the pB (cis) forms of the proteins at 20°C.}$

Protein	in TAE, pH 7.5, 100 mM NaCl	+ non-specific DNA	+ non-specific DNA & equimolar AP-1 DNA	Fold change (+ AP-1)
GCN4Δ25PYP-v2	99 ± 3	80 ± 3 s	476 ± 20	5.9
Δ25ΡΥΡ	212 ± 6	225 ± 5	225 ± 5	1
G54A	221 ± 6	$150 \pm 4 \text{ s}$	552 ± 20	3.7
G54E	137 ± 4	$100 \pm 3 \text{ s}$	349 ± 15	3.5
K143I	91 ± 3	87 ± 7	740 ± 20	8.5
K143F	96 ± 3	132 ± 3	1189 ± 60	9
G54E-K143I	54 ± 4	60 ± 5	565 ± 20	9.4
E35M-G54E-K143I	92 ± 4	122 ± 5	724 ± 20	5.9
E35M-G54E-K143F	68 ± 2	144 ± 4	771 ± 15	5.4
E45K-G54E-K143I	243 ± 5	684 ± 15	882 ± 20	1.3
E35M-E45K-G54E-K143I	215 ± 6	325 ± 15	700 ± 20	2.1

 Table 5

 Specific AP-1 DNA apparent binding affinities of the proteins in dark-adapted and irradiated states.

Protein	K _d app dark-adapted (nM)	K _d app irradiated (nM)	$K_{d}app(dark)/K_{d}app(light)$	Max fold increase in % DNA bound
GCN4Δ25PYP-v2	571 ± 17	297 ± 11	1.9	3.6
G54A	528 ± 16	356 ± 15	1.5	2.3
G54E	717 ± 15	392 ± 15	1.8	3.2
K143I	635 ± 15	264 ± 11	2.4	5.8
K143F	383 ± 13	108 ± 8	3.5	12
G54E-K143I	301 ± 15	119 ± 8	2.5	6.3
E35M-G54E-K143I	305 ± 16	166 ± 10	1.8	3.2
E35M-G54E-K143F	165 ± 6	74 ± 6	2.2	4.8
E45K-G54E-K143I	121 ± 10	120 ± 10	1.0	1.0
E35M-E45K-G54E-K143I	159 ± 11	134 ± 10	1.2	1.4